

Phonon Knudsen flow in nanostructured semiconductor systems

E. Ziambaras and P. Hyldgaard

*Department of Applied Physics, Chalmers University
of Technology, SE-412 96 Göteborg, Sweden*

(Dated: November 1, 2018)

Abstract

We determine the size effect on the lattice thermal conductivity of nanoscale wire and multilayer structures formed in and by some typical semiconductor materials, using the Boltzmann transport equation and focusing on the Knudsen flow effect. For both types of nanostructured systems we find that the phonon transport is reduced significantly below the bulk value by boundary scattering off interface defects and/or interface modes. The Knudsen flow effects are important for almost all types of semiconductor nanostructures but we find them most pronounced in Si and SiC systems due to the very large phonon mean-free paths. We apply and test our wire thermal-transport results to recent measurements on Si nanowires. We further investigate and predict size effects in typical multilayered SiC nanostructures, for example, a doped-SiC/SiC/SiO₂ layered structure that could define the transport channel in a nanosize transistor. Here the phonon-interface scattering produces a heterostructure thermal conductivity smaller than what is predicted in a traditional heat-transport calculation, suggesting a breakdown of the traditional Fourier analysis even at room temperatures. Finally, we show that the effective thermal transport in a SiC/SiO₂ heterostructure is sensitive to the oxide depth and could thus be used as an in-situ probe of the SiC oxidation progress.

PACS numbers: 44.05.+e, 44.10.+i, 66.70.+f

I. INTRODUCTION

Thermal transport in nanostructured semiconductor systems is important for the continued development of nanoscale electronics.^{1,2} A number of recent experimental^{3,4,5,6,7,8,9} and theoretical^{10,11,12,13,14,15,16,17,18,19,20,21,22,23,24,25,26,27,28,29,30,31,32,33,34,35} studies contributes to an emerging understanding of interesting science issues and potential technology problems. Opto- and power-electronics devices generate significant heat that must be dissipated to avoid degradation of the device performance,^{2,36} and similar problems increasingly affect also more standard electronics applications.

The thermal transport in semiconductor structures is dominated by phonons and measurements on bulk samples would indicate excellent thermal transport properties due to the material hardness and purity. However, typical device designs involve necessary nanostructuring, for example, the construction of material heterostructures that define quantum wells or traps a transport channel below an oxide and above a doped substrate. The associated formation of interfaces is documented to effectively suppress the thermal transport both parallel^{3,4,5,6,10,11,12,13,14,15,16,17,18,19,20,21,22,23,24,25,26} and perpendicular^{9,27,28,29,30,31,32,33,34,35} to the materials boundaries due to the phonon Knudsen flow^{10,11,15,37,38} and the phonon reflection^{6,12,28,29,34} effects, respectively. Both types of interface mechanisms lie outside the traditional Fourier analysis³⁹ of heat conduction but produce a suppression of the effective thermal conductivity within a region extending to about one phonon mean-free path ℓ_{mfp} from the interface. The interface impact of scattering can even cause crossovers in the nanostructure conductivity such that a material with high bulk thermal conductivity is not necessarily the best thermal conductor upon nanostructuring.²¹ While thermal-conductivity suppressions can work to improve the efficiency of both thermoelectric and thermoionic cooling,^{1,40,41,42,43,44,45,46} room-temperature estimates,⁴⁷ $\ell_{\text{mfp}}(T = 300\text{K}) \geq 100 \text{ nm}$, also testifies to some adverse effects even for present devices. Worse, the quest to nanosize modern electronics can only exacerbate the thermal dissipation problems^{2,36} since the increase in packing density simultaneously will produce a further degradation in the effective thermal-transport properties.

In this paper we illustrate the general nature of this Knudsen effect on the effective lattice thermal conductivity of semiconductor devices by documenting the effects on two simple sample structures: thin semiconducting wire^{3,15,16,17,19,20,21,48} and multilayered

systems,^{4,5,6,7,10,11,12,13,14,35,47} Fig. 1. Semiconductor wires and layers represent examples of semiconductor nanostructures that are interesting in themselves. They can also be viewed as typical building blocks in general semiconducting devices that typically have transport channels sandwiched between an oxide and substrate.

Figure 1 shows schematics of both types of nanostructures; the light regions in the schematics represent the transport active systems of high thermal conductivity while the dark regions illustrate the processed surrounding which may be oxides or heavily doped materials. In both systems the oxide or the dopants will inhibit or limit the thermal transport in the processed regions and move the phonon transport to the transport active wire or layer. However, the interface scattering suppresses the thermal transport even in the (pure) transport channel where the scattering causes a Knudsen flow.^{37,38}

We obtain analytical results for the thermal-transport suppression given by special functions in both the wire and (multi)layer cases. The analytical results hold exactly when the phonon mean-free path ℓ_{mfp} can be approximated as constant⁴⁹ and simplify the thermal-transport calculations for wires and multilayers to simple frequency integrals in the more general case when ℓ_{mfp} depends on mode 'i' and momentum 'q'. We thus extend previous investigations^{4,10,11,12,13,15,18,19,35} by efficient evaluations of the wire and layer thermal conductivities κ_{wire} , κ_{layer} , and by (analytical) results for the layer Knudsen flow that arises when the nature of interface scattering differs at the two materials boundaries in a multilayer structure. These results also permit an efficient evaluation of the multilayer thermal transport. We find that the Knudsen flow effect³⁸ is important in nanosized wires and multilayered structures formed from typical semiconductor materials due to the very large phonon mean-free paths. We test the accuracy of the approximations used to calculate the phonon Knudsen flow by comparing our results to experimental measurements for a nanosized Si wire.³ We further investigate the phonon Knudsen flow in typical multilayer structures, including a simplified model of a nanosize transistor transport channel,⁴⁷ and demonstrate a breakdown of the traditional Fourier analysis³⁹ for some semiconductor nanostructures at and below room temperature. Finally we suggest an indirect but in-situ probe⁴⁷ for the oxidation progress in SiC (and Si) materials.

Figure 2 summarizes the predicted suppression in the lattice thermal conductivity of general semiconductor wire and layer nanostructures. We stress that there is a difference in thermal-conductivity range used to present the results for SiC, Si, and GaAs materials

but that the overall physical behavior and consequences for semiconductor nanostructures remain unchanged in all materials. The *left* panels show κ_{wire} (dashed curves) and κ_{layer} (solid curves) for varying thickness $d_{\text{wire, layer}}$ for SiC, Si, and GaAs at $T = 300$ K. The dotted lines identify the experimentally observed value of the bulk-material thermal conductivities from which we also extract the listed values of the phonon mean-free paths ℓ_{mfp} . The *top right* and *middle right* panels document the temperature variation in the Knudsen-flow thermal conductivity in SiC and Si layers (solid curves) and wires (dashed curves). Finally, the *lower right* panel shows the calculated temperature variation in the phonon mean-free path $\ell_{\text{mfp}}(T)$ for SiC, Si, and GaAs. The phonon Knudsen-flow effect on the thermal transport arises because this $\ell_{\text{mfp}}(T)$ approaches the microscale at lower temperatures and may even at room temperature exceed the typical separation between boundaries in modern and future semiconductor devices.

This paper is organized as follows. In section II we estimate the bulk-phonon mean-free path in SiC, Si, and GaAs, and we discuss the general Knudsen-flow behavior in low-dimensional systems. In section III we analyze the phonon-boundary scattering in wires and layered structures and we present complete special-function evaluations^{47,50,51} for the lattice thermal conductivities κ_{wire} and κ_{layer} . In section IV we discuss and compare the present approach with traditional thermal transport calculations of low-dimensional systems, and we suggest a possible in-situ probe of the SiC oxidation process. Finally, section V contains our conclusions.

II. PHONON TRANSPORT THEORY

We investigate the thermal transport properties in semiconductors where the dominant heat carriers are the phonons. For every phonon momentum q (and phonon mode i) we determine the distribution function $N_{q(i)}$ which relaxes to an equilibrium value, $N_{q(i)}^0 = 1/[\exp(\hbar\omega_q^{(i)}/k_B T) - 1]$, given exclusively by the temperature T and the phonon energy $\hbar\omega_q^{(i)}$ of said mode. We use a relaxation time $\tau_q^{(i)}$ to describe the effective scattering in the bulk material. Further, we ignore the optical modes and assume for the longitudinal and transverse modes^{52,53} ($i = l, t$) a simple isotropic phonon dispersion given by $q = \omega(1 + \alpha_i \omega^3)/c_i$ and parameters α_i fitted to the phonon energies at the zone boundaries Θ_i .⁵⁴ Table I lists the sound velocities, c_i , and effective Debye temperatures, Θ_i , for SiC, Si, GaAs,

and Ge along with the fitted values for the dispersion parameter α_i .

We mostly focus on the case with a constant, effective phonon mean-free path ℓ_{mfp} (that only depends on temperature and materials) but we also provide results and analysis for the more general case of a (mode- and) momentum-dependent mean-free path $\ell_{\text{mfp}}^{(i)}(q) = v_q^{(i)} t_q^{(i)}$. We use our model of the phonon dynamics to estimate the group velocities $v_q^{(i)} = c_i/(1 + 4\alpha_i\omega^3)$. In the following derivation and discussion we generally suppress the explicit labeling by mode index but all calculations have been performed by handling the longitudinal and transverse phonon modes separately.

The distribution change $\delta N_q = N_q - N_q^0$ induced by a small thermal gradient, ∇T , is calculated by solving the Boltzmann transport equation in the relaxation-time approximation,⁵⁵

$$(\mathbf{v}_q \cdot \nabla) N_q = -\frac{N_q - N_q^0}{\tau_q}, \quad (1)$$

to linear order in the thermal gradient ∇T . The q (mode) dependent value of the relaxation rate $1/\tau_q$ is effectively fitted from bulk-thermal transport measurements^{52,56} as discussed below. In turn, the calculated distribution change δN_q permits our evaluation of the thermal current

$$\mathbf{j} = \sum_i \int \frac{d^3q}{(2\pi)^3} \hbar \omega_q^i \mathbf{v}_q^i \delta N_{qi}, \quad (2)$$

and hence of the thermal conductivity

$$\kappa = -\mathbf{j}(\nabla T)^{-1}. \quad (3)$$

The interface scattering enters from the proper inclusion of the boundary conditions in Eq. (1).

II A. Estimate of the phonon mean-free path in bulk

To obtain an approximate evaluation of the phonon mean-free path we first consider the thermal transport in a bulk material where the solution of the linearized Boltzmann transport equation (l-BTE) simplifies to

$$\delta N_{q(i)}^{\text{Bulk}} = -\tau_q^{(i)} (\mathbf{v}_q^{(i)} \cdot \nabla T) \left(\frac{\partial N_{q(i)}^0}{\partial T} \right). \quad (4)$$

The lattice thermal conductivity, κ_{Bulk} , is calculated by inserting this solution in Eqs. (2) and (3). For a frequency and polarization-independent phonon mean-free path, $\tau_q^{(i)} v_q^{(i)} \equiv$

$\ell_{\text{mfp}}(T)$, the lattice thermal conductivity in a bulk material $\kappa_{\text{Bulk}} \propto \ell_{\text{mfp}}$ is simply proportional to this effective mean-free path.^{11,15} Comparison to experimental values for the temperature variation in the bulk thermal conductivities, $\kappa_{\text{Bulk}}^{\text{exp}}(T)$, therefore yields a simple phonon mean-free path estimate^{11,15}

$$\ell_{\text{mfp}}(T) = \kappa_{\text{Bulk}}^{\text{exp}}(T) \frac{6\pi^2 \hbar^3}{k_B^4 T^3} \left(\frac{2f_t(T)}{c_t^2} + \frac{f_l(T)}{c_l^2} \right)^{-1}. \quad (5)$$

The estimate depends on the modal dispersion as expressed through the occupation-weighted integrals

$$f_i(T) = \int_0^{\Theta_i/T} dx \frac{x^4 e^x}{(e^x - 1)^2} \left[1 + \alpha_i \left(\frac{x k_B T}{\hbar} \right)^3 \right]^2. \quad (6)$$

The *lower right* panel of figure 2 shows the calculated variation of the phonon mean-free path ℓ_{mfp} as a function of the temperature for the set of semiconducting materials studied. For GaAs and Ge we use values of $\kappa_{\text{Bulk}}^{\text{exp}}$ taken from Ref. 52 while for SiC and Si we use values from Ref. 56. The corresponding curve for Ge coincides almost exactly with that for GaAs because of the similarity in sound velocities and in measured values for the bulk thermal conductivities. We note that the phonon mean-free paths in the three materials are almost of micron-scale dimensions and that SiC possesses the largest value of ℓ_{mfp} ($\ell_{\text{mfp}}^{\text{SiC}} \approx 1.5 \ell_{\text{mfp}}^{\text{Si}} \approx 3 \ell_{\text{mfp}}^{\text{Ge, GaAs}}$).

Our approximative constant- ℓ_{mfp} description provides simple and analytical evaluations of the Knudsen thermal-transport suppression in both the wire and multilayer cases. This description permits qualitative estimates of the general effect.⁴⁹ The actual bulk-phonon mean-free path $\ell_{\text{mfp}}^{(i)}(q) = \tau_q^{(i)} v_q^{(i)}$ will, of course, depend on the mode and on the phonon momentum q and/or the frequency $\omega_q^{(i)}$ and calls for a more refined analysis. We test the validity of the constant- ℓ_{mfp} results by also considering the Knudsen flow arising with a frequency-dependent (mode-independent) effective decay rate¹⁵ $\tau = A(T)/\omega^2$ and by comparing the results of both theory descriptions to recent experimental observations of the thermal transport in Si nanowires.³ For the test model we determine the function $A(T)$ from measurements⁵⁶ of the temperature variation of the bulk (Si) thermal conductivity using

$$A(T) = \kappa_{\text{Bulk}}^{\text{exp}}(T) \frac{6\pi^2 \hbar}{k_B^2 T} \left(\frac{2g_t(T)}{c_t} + \frac{g_l(T)}{c_l} \right)^{-1}, \quad (7)$$

where the functions g_i are defined as

$$g_i(T) = \int_0^{\Theta_i/T} dx \frac{x^4 e^x}{(e^x - 1)^2} \frac{[1 + \alpha_i(xk_B T/\hbar)^3]^2}{[1 + 4\alpha_i(xk_B T/\hbar)^3]}. \quad (8)$$

In this more refined model description we determine below the Knudsen suppression analytically up to a single integration over the phonon frequency.

II B. Phonon Knudsen flow

We focus our study of the Knudsen flow effect on two types of nanosized semiconductor structures that can be viewed as general building blocks in devices. The *upper panel of Fig. 1* illustrates two possible realizations of wire systems^{3,9,15,48} which could be embedded in an oxide or could exist as a free-standing object. The phonons are assumed to undergo either specular or diffusive scattering with the probability p and $1 - p$ at the wire boundary. The *lower panel of Fig. 1* shows a corresponding realization of a multilayer structure in which the transport-active channel (of high material purity) is located between two similar or different materials representing, for example, an oxide cap and a highly doped substrate. The surrounding materials (and/or vacuum) suppress the average transport not only because they have inferior conductivities themselves but also because their material boundaries cause a Knudsen-flow suppression even in the transport channel. Again, two types of scattering events are possible and phonons are assumed to scatter specularly from the upper (lower) interface with probability $p_{+(-)}$ and diffusively with probability $1 - p_{+(-)}$, respectively. The value of p_+ will generally differ from p_- as, for example, an oxide interface is rough ($p_+ = 0$) whereas the interface to an underlying (doped or undoped) substrate may be very smooth ($p_- \rightarrow 1$).

The phonon-boundary scattering off interface/surface defects becomes dominant when the phonon mean-free path exceeds the dimensions of the material.^{10,11,15,38} To analyze the general situation we introduce q_\perp (q_\parallel) to denote the component of the phonon momentum q that is perpendicular to the material boundary Ω (parallel to the thermal gradient, ∇T). Specular phonon scattering has only indirect effects on the overall transport because the phonons will have the same momentum component q_\parallel in the direction of the thermal gradient ∇T as before the scattering event. For such specular scattering we have

$$\delta N_q(\Omega, q_\perp) = \delta N_q(\Omega, -q_\perp). \quad (9)$$

In contrast, diffusive interface scattering causes a significant transport suppression as the phonon emerges with a random direction given by the local thermal distribution. The implicit thermalization ensures

$$\delta N_q(\Omega, q_\perp > 0) = 0, \quad (10)$$

and this boundary condition affects the distribution also away from the interface.

To calculate the resulting impact on the thermal transport for our low-dimensional structures we solve the l-BTE

$$\left\{ \frac{1}{q} (q_\perp \cdot \nabla) + \frac{1}{\tau_q v_q} \right\} \delta N_q = -\frac{1}{q} \frac{\partial N_q^0}{\partial T} (q_\parallel \cdot \nabla T) \quad (11)$$

subject to the boundary conditions Eqs. (9) and (10). We express the general solution relative to the corresponding bulk case

$$\delta N_q = \delta N_q^{\text{Bulk}} [1 - h_q(r_\perp, q_\perp/q, p)] \quad (12)$$

using r_\perp to denote the coordinate direction away from the local surface. Furthermore, the form of the l-BTE (11) permits us to express the relative suppression in terms of an amplitude $\phi_q(q_\perp/q, p) > 0$ and an exponential decay

$$h_q(r_\perp, q_\perp/q, p) = \phi_q(q_\perp/q, p) e^{-r_\perp / \{\tau_q v_q (q_\perp/q)\}}. \quad (13)$$

The amplitudes $\phi_q(q_\perp/q, p)$ are fixed by analysis of the boundary conditions.^{15,37,50,51}

Figure 3 illustrates the general nature of the Knudsen flow in the phonon distribution, $\delta N_q / \delta N_q^{\text{Bulk}}$, as functions of the momentum angle q_\perp/q (top panel) and of the spatial coordinate x across the diameter (bottom panel). The Knudsen-flow distribution δN_q is specified by numerical integration^{13,15,19} and/or analytical evaluation.^{11,47,50,51} The figure details the variation in $\delta N_q / \delta N_q^{\text{Bulk}}$ and compares results obtained assuming purely diffusive scattering ($p = 0$) for two wires with diameters $d_{\text{wire}} = \ell_{\text{mfp}}^{(i)}(q)$ and $2\ell_{\text{mfp}}^{(i)}(q)$. The calculated suppression applies for all phonon momenta (and modes) for wires when, as we typically do, we approximate the phonon mean-free path as constant. More generally, the figure illustrates the universal effect in the Knudsen flow with a suppression of distribution changes extending far away from the boundaries; similar momentum and spatial variation curves result both under more general assumptions for the mean-free path and in the case of multilayered semiconductor nanostructures.

The resulting effect on the thermal conductivity κ can be summarized by averaging the relative suppression $h_{q(i)}$ over the cross section (perpendicular to ∇T). For every phonon q and i we define $\mathcal{H}_{qi}(q_{\perp}/q, p) = \int_{\Gamma} d\Gamma h_{qi}(r_{\perp}, q_{\perp}/q, p)/\Gamma$ and express the nanostructure conductivity change

$$\delta\kappa = \kappa - \kappa_{\text{Bulk}} = (\nabla T)^{-1} \sum_i \int \frac{d^3q}{(2\pi)^3} \hbar\omega_q^i v_q^i \frac{q_{\parallel}}{q} \delta N_{qi}^{\text{Bulk}} \mathcal{H}_{qi}(q_{\perp}/q, p). \quad (14)$$

It is convenient to introduce an effective inverse Knudsen number $\eta_i(q) = d_{\text{wire(layer)}}/(\tau_q^i v_q^i)$ and describe the thermal-conductivity suppression¹⁵

$$-\frac{\delta\kappa}{\kappa_{\text{Bulk}}}(p) = \frac{\sum_i \int_0^{\Theta_i/T} dx x^4 e^x (e^x - 1)^{-2} [1 + \alpha_i(xk_B T/\hbar)^3]^2 F_{qi}(p)|_{\eta_i(q(x))}}{\sum_i \int_0^{\Theta_i/T} dx x^4 e^x (e^x - 1)^{-2} [1 + \alpha_i(xk_B T/\hbar)^3]^2} \quad (15)$$

as a weighted frequency integral over the effective suppression factor

$$F_{qi}(p)|_{\eta_i(q)} \equiv \left(\frac{4\pi}{3}\right)^{-1} \int_{|\vec{q}|=q} d^2q \left(\frac{q_{\parallel}}{q}\right)^2 \mathcal{H}_{qi}(q_{\perp}/q, p). \quad (16)$$

We emphasize that significant simplification follows from an assumption of a mode and frequency independent $\ell_{\text{mfp}} = \text{constant}$. In that case we obtain the simple result^{10,11,15,19}

$$-\frac{\delta\kappa}{\kappa_{\text{Bulk}}}(\eta = \text{constant}, p) = F_{qi}(p)|_{\eta_i(q)=\eta} \quad (17)$$

for the Knudsen effect on the nanostructure thermal transport. This follows because the value of η is then independent of q and of the mode. For the case of wires and multilayered structures it is possible to obtain analytical results for the solution (17).

III. INTERFACE-LIMITED NANOSTRUCTURES THERMAL TRANSPORT

The study of the thermal transport in wires and layered structures requires a careful analysis³⁷ of the phonon scattering at the interfaces of the specific systems. From this analysis we can complete the evaluation of the Knudsen transport suppression (17) for a free-standing wire, for a individual layer with possibly different nature of scattering at the top and bottom interfaces, and for a multilayered structure. Details of the derivation is published elsewhere^{50,51} and here we just summarize the approach and the analytical results obtained.⁴⁷

III A. Thermal conductivity in wires

For a free standing wire (Figure 1) we assume a thermal gradient along the wire-axis 'z'. For simplicity we let the x -direction coincide with the perpendicular phonon momentum, *i.e.*, $q_{\perp} = q_x$, and we assume the same specular scattering ratio p along the whole boundary. Under these conditions we solve the l-BTE (Eq. (11)) for the change δN^{wire} subject to the boundary conditions (9) and (10) with $\Omega_+ = \sqrt{(d/2)^2 - y^2}$ for $x > 0$ and $\Omega_- = -\sqrt{(d/2)^2 - y^2}$ for $x < 0$. We analyze the boundary effect following Ref. 37, adapting^{15,50} the description originally developed for electron transport in thin films.

Using the definition (12) we formally determine the wire suppression ratio

$$h_q^{\text{wire}}(x, y, q_x/q, p) = (1-p) \frac{\exp(-\sqrt{(d/2)^2 - y^2}/\{\tau_q v_q(q_x/q)\})}{1-p \exp(-2\sqrt{(d/2)^2 - y^2}/\{\tau_q v_q(q_x/q)\})} e^{-x/\{\tau_q v_q(q_x/q)\}} \quad (18)$$

and evaluate the average amplitude suppression^{15,50}

$$\mathcal{H}_q^{\text{wire}}(q_{\perp}, /q, p) = \frac{4}{\pi} (1-p)^2 \sum_{j=1}^{\infty} j p^{j-1} \int_0^1 dt \sqrt{1-t^2} e^{-jt\eta(q)/(q_{\perp}/q)}. \quad (19)$$

A polar coordinate system, where $q_x = q \sin \theta$, is then used to express the weighted Knudsen suppression factor (16) at mode i ,

$$\begin{aligned} F_{qi}^{\text{wire}}(p)|_{\eta_i(q)} &= \left(\frac{4\pi}{3}\right)^{-1} \int_0^{2\pi} d\varphi \int_0^{\pi} d\theta \sin \theta \cos^2 \theta \mathcal{H}_{qi}^{\text{wire}}(q_x/q = \sin \theta; p) \\ &= (1-p)^2 \sum_{j=1}^{\infty} j p^{j-1} M(j\eta), \end{aligned} \quad (20)$$

in terms of a Meijer's G special function⁵⁷ and a polynomial:

$$M(\zeta) = \frac{6}{\zeta} \left\{ \frac{\pi^{3/2}}{4} G_{24}^{20} \left(\begin{matrix} \zeta^2 \\ 4 \end{matrix} \middle| \begin{matrix} 1, 3 \\ \frac{1}{2}, \frac{3}{2}, -\frac{1}{2}, 1 \end{matrix} \right) - \left(\frac{\zeta^2}{6} - \frac{\zeta^4}{45} \right) \right\}. \quad (21)$$

For purely diffusive scattering ($p \rightarrow 0$) only the first term in the sum of Eq. (20) contributes to the lattice thermal conductivity and therefore the ratio $\kappa_{\text{wire}}/\kappa_{\text{Bulk}}$ simplifies to

$$\frac{\kappa_{\text{wire}}}{\kappa_{\text{Bulk}}}(\eta, p \rightarrow 0) = 1 - \frac{6}{\eta} \left\{ \frac{\pi^{3/2}}{4} G_{24}^{20} \left(\begin{matrix} \eta^2 \\ 4 \end{matrix} \middle| \begin{matrix} 1, 3 \\ \frac{1}{2}, \frac{3}{2}, -\frac{1}{2}, 1 \end{matrix} \right) - \frac{\eta^2}{6} + \frac{\eta^4}{45} \right\}. \quad (22)$$

Similarly, if instead we assume pure specular scattering along the whole wire-boundary then $F^{\text{wire}}(p \rightarrow 1)|_{\eta} \rightarrow 0$ so that the bulk transport description is correctly recovered.

Our analytical results (20)–(21) and/or (22) are in exact agreement with the numerical results⁵⁸ presented in Ref. 15. Our analytical l-BTE result differs quantitatively but not qualitatively from the nonselfconsistent κ_{wire} determination^{18,59} that can be extracted from analytical calculations of how boundary scattering shortens the average phonon mean-free path.¹⁸ We stress that our results (20)–(21) and/or (22) completes the previously published investigation¹⁵ by a special function evaluation for a significant speed up in computation efficiency. We also stress that care must be taken in the numerical evaluation of our special function (21), or the integral in Eq. (20) for large arguments ($\zeta > 10$) when using, for example, the Mathematica program.

III B. Thermal conductivity in an individual layer

We consider a layer of thickness d with its boundaries at $z = \pm d/2$ and a thermal gradient lying in the xy -plane. In this geometry we have $q_{\perp} = q_z$. In the general case, $p_+ \neq p_-$, we must analyze the phonon scattering at both interfaces in order to evaluate the induced change, $\delta N_q^{\text{layer}}$. Generalizing previous results^{10,11,15,37,38} and introducing $\eta = d_{\text{layer}}/\ell_{\text{mfp}}$ and $\xi = \eta/(2|q_z|/q)$, we obtain for general $p_{+/-}$ the result^{50,51}

$$\begin{pmatrix} \phi_{q,q_z>0}^{\text{layer}}(p_+, p_-) \\ \phi_{q,q_z<0}^{\text{layer}}(p_+, p_-) \end{pmatrix} = \frac{1}{e^{2\xi} - p_- p_+ e^{-2\xi}} \begin{pmatrix} (p_- - 1)e^{\xi} + p_-(p_+ - 1)e^{-\xi} \\ (p_+ - 1)e^{\xi} + p_+(p_- - 1)e^{-\xi} \end{pmatrix}, \quad (23)$$

for the amplitudes of the suppression caused by scattering at the upper and lower interfaces.

For our single-layer and multilayer calculations we will generally assume that we have a constant ℓ_{mfp} and can hence express the Knudsen transport suppression

$$\frac{\kappa_{\text{layer}}}{\kappa_{\text{Bulk}}}(\eta, p) = 1 - F^{\text{layer}}(p_+, p_-)|_{\eta=\text{constant}}; \quad (24)$$

generalizations to a mode and frequency-dependent phonon mean-free path are as straightforward as in the wire case. We calculate again the cross-section average of the distributions change, $\mathcal{H}_q^{\text{layer}}(q_z/q; p_+, p_-)$, and determine the phonon suppression factor as an average over the direction of momentum q

$$F^{\text{layer}}(p_+, p_-)|_{\eta=\text{constant}} = \frac{3}{4} \int_0^{\pi} d\theta \sin^3 \theta \mathcal{H}_q^{\text{layer}} \left(\frac{q_{\perp}}{q} = \cos \theta; p_+, p_- \right), \quad (25)$$

noting that the sign of $\cos(\theta) = q_{\perp}/q = q_z/q$ uniquely determines whether the emerging phonons have scattered off the top or bottom material boundary.⁵⁰ Introducing finally

$$\bar{p} = \frac{p_+ + p_-}{2} \quad \text{and} \quad \hat{p} = \sqrt{p_+ p_-}. \quad (26)$$

and performing the θ -integration we obtain the analytical result^{47,50,51}

$$F^{\text{layer}}(\bar{p}, \hat{p})|_{\eta=\text{constant}} = \frac{3}{8\eta} \left\{ (1 - \bar{p}) - 4 \sum_{j=1}^{\infty} Q(j, \eta, \bar{p}, \hat{p}) \right\}, \quad (27)$$

given in terms of a modified exponential error function

$$Q(j, \eta, \bar{p}, \hat{p}) = (\hat{p}^2 - 2\bar{p} + 1)\hat{p}^{j-1}D(j\eta) + (\bar{p} - \hat{p})(\hat{p} + 1)^2\hat{p}^{2(j-1)}D(2j\eta), \quad (28)$$

where

$$D(a\eta) = \left(\frac{1}{4} - 5\frac{a\eta}{12} - \frac{(a\eta)^2}{24} + \frac{(a\eta)^3}{24} \right) e^{-a\eta} + \left(\frac{(a\eta)^2}{2} - \frac{(a\eta)^4}{24} \right) \int_{\eta}^{\infty} dk \frac{e^{-ak}}{k}. \quad (29)$$

At $p_+ = p_-$ the present more general result (27)-(29) correctly simplifies to

$$\frac{\kappa_{\text{layer}}}{\kappa_{\text{Bulk}}}(\eta, p) = 1 - (1 - p)\frac{3}{8\eta} \left\{ 1 - 4(1 - p) \sum_{j=1}^{\infty} p^{j-1}D(j\eta) \right\}, \quad (30)$$

as obtained in previous derivations.^{10,11,15,32}

Figure 4 shows the reduction of the lattice thermal conductivity in pure semiconductor layers. The *top* panel documents the ratio $\kappa_{\text{layer}}/\kappa_{\text{Bulk}}$ as a function of $\eta \equiv d_{\text{layer}}/\ell_{\text{mfp}}$ for $p_+ = p_- = p$. As in the wire case, the lattice thermal conductivity naturally becomes higher to recover the bulk behavior when the probability for specular scattering increases. The *lower* panel shows $\kappa_{\text{layer}}/\kappa_{\text{Bulk}}$ for a fixed layer-thickness $d_{\text{layer}} = 0.1\ell_{\text{mfp}}$ and for varying specular scattering probabilities, p_+ and p_- . The figure documents that the thermal conductivity remains suppressed below the bulk transport value even when the phonons are purely specularly scattered from one of the two interfaces.

III C. Thermal transport in multilayered structures

To estimate the thermal transport in heterostructures we make the approximation to ignore all phonon transmission between the layers. There exists exact results¹³ but our focus

is on providing simple estimates and extracting consequences of the size-limited thermal transport. We consider structures with layers $j = 1, 2 \dots$ of individual thicknesses d_j and with probabilities $p_{+(-)}^j$ for specular (rather than diffusive) scattering at the top (bottom) layer boundary. Our approximation then consists in approximating the effective (linear-response) conductivity as

$$\kappa_{\text{eff}} = \frac{\sum_j \kappa_j(d_j, p_+^j, p_-^j) d_j}{\sum_j d_j}, \quad (31)$$

where $\kappa_j(d_j, p_+^j, p_-^j)$ denotes the thermal conductivity of layer j . We stress that the individual-layer thermal conductivity typically is subject to a significant Knudsen-flow suppression and must be calculated for the layer-specific nature of the boundary scattering ($p_{+/-}^j$) and for the specific individual-layer thickness d_j , as also indicated by the argument to the individual-layer conductivities κ_j .

IV. RESULTS AND DISCUSSION

The Knudsen flow effect has direct consequences for the semiconductor nanostructure thermal transport. Below we test the accuracy of our approximations and detail the size effects on the temperature variation of κ_{wire} and κ_{layer} .

IV A. Thermal transport in Si and SiC nanostructures

Figure 5 tests the accuracy of our approximative determination of the Knudsen flow effects by comparing the measured³ and calculated temperature variation of the lattice thermal conductivity in a 115 nm thick silicon wire. The solid circles represent experimental data from Ref. 3 while the solid (dashed) curve shows our theoretical results (20)–(21), (22) for the Knudsen flow calculated for pure diffusive scattering ($p = 0$) and assuming a frequency and polarization-independent bulk-phonon mean-free path ℓ_{mfp} (a frequency-dependent relaxation time¹⁵ $\tau_q = A(T)/\omega_q^2$ using (7)–(8) to calculate the function $A(T)$). The insert compares the predicted Si wire thermal conductivity with measurements⁵⁶ of bulk Si on logarithmic scales, emphasizing the significant effects of nanostructuring.

The figure reveals some discrepancies which we assign to the simple approximation we use for the phonon dispersion.¹⁶ The figure also shows that the more elaborate model with a frequency dependent τ and ℓ_{mfp} yields the more accurate description. However, since these

two models give similar magnitude and qualitative behavior of κ_{wire} (with good agreement to the measured values) we find that the analytical result (22) serves as a simple, analytical estimate of the wire conductivity κ_{wire} .

Figure 6 compares the corresponding thermal-conductivity variation with temperature of bulk SiC (dashed-dotted curve) and of a 115 nm thick SiC wire (dashed curve) and layer (solid curve) structure. For both nanostructures we assume pure diffusive scattering ($p = 0$) at all interfaces and a frequency and mode-independent bulk-phonon mean-free path described by Eq. (5).

Together the insert of Fig. 5 and Fig. 6 stress the two features which are important when studying the thermal transport in nanostructure (Si and SiC) systems:^{3,16} (i) the maximum bulk-transport value is about two orders of magnitude higher than the corresponding peak values for the nanostructures, *i.e.*, $\kappa_{\text{Bulk}}^{\text{max}}(T) \approx 100\kappa_{\text{layer, wire}}^{\text{max}}(T)$, and (ii) the maximum values of the lattice thermal conductivity in the wires and layers are shifted towards higher temperatures from the peak of the bulk conductivities.

IV B. Thermal transport in doped materials

Figure 7 documents that the Knudsen suppression in the lattice thermal conductivity also affects the case of doped Si and SiC nanostructures. The figure compares the conductivity of a Si and SiC layer at two different temperatures, 77 K and 300 K for pure materials (solid curves) and in the case of a very high dopant concentration $\sim 10^{20} \text{ cm}^{-3}$ (dashed curves). We assume here that the phonons are scattered purely diffusively at both interfaces ($p_+ = p_- = 0$) and use the analytical result (27)–(29) for an assumed constant $\ell_{\text{mfp}}(T)$. We use the measurements of Ref. 56 with the Si layer p-doped to be $1.7 \cdot 10^{20} \text{ cm}^{-3}$ and the SiC layer n-doped $5 \cdot 10^{19} \text{ cm}^{-3}$. The phonon mean-free path in the doped layers is thus estimated at room temperature to be 49 nm and 138 nm for SiC and Si, respectively and at $T = 77 \text{ K}$ to be 420 nm and 830 nm, respectively.

IV C. Breakdown of Fourier transport analysis

Figure 8 documents that traditional thermal transport calculations fail to accurately describe the phonon transport in low-dimensional systems at and below room temperature.

This is illustrated for a $\text{SiO}_2/\text{SiC}/\text{SiO}_2$ heterostructure for which we have calculated the effective multilayer thermal conductivity (31) for varying thickness of the SiC layer, d_{SiC} . At the SiC/SiO₂ interface we assume pure diffusive phonon scattering ($p = 0$). The solid curve represents the effective lattice thermal conductivity obtained by the present Knudsen approach (described in Sec. III B) in which the thermal-conductivity suppression in each individual layer is considered. In contrast, the dashed curve was obtained by replacing the suppressed value of the layer conductivity in Eq. (31) by the corresponding bulk transport conductivity, as is typically done in many finite element calculations. This Fourier analysis yields an effective lattice thermal conductivity which is too large. Traditional Fourier analysis³⁹ of the lattice thermal transport is inadequate for some nanostructured semiconductor systems in the low-temperature regime and the Knudsen-flow suppression affects even the room-temperature behavior.

IV D. SiC oxidation

Figure 9 illustrates the use of the Knudsen–flow thermal transport as a possible gauge of the SiC oxidation process. Metal-oxide-semiconductor transistor gates are usually formed by oxidizing the Si to form a thin oxide film⁶⁰ located on top of the pure transport channel. This has been the focus of many experimental and theoretical investigations.^{61,62,63,64,65,66} Many of the experimental probes require that one extracts the sample and investigate it in, for example, a transmission electron microscope whereas qualitative in-situ probes could be more useful for some applications. We note that the SiC/SiO₂ interface is rough but of relative uniform thickness.⁶⁵ The situation is similar to the case of adsorption on metal films where the (electrical) conductance is proven to be sensitive^{67,68,69,70,71,72} to the film thickness and surface nature. We therefore argue⁴⁷ that measurements of the thermal Knudsen flow could serve as such an in-situ probe of the oxidation progress.^{61,62,63,64,65,66}

The figure shows the variation of the effective lattice thermal conductivity, κ_{eff} , with the oxide-thickness, d_{SiO_2} , calculated by Eq. (31). We use the value⁷³ $1.4 \text{ W m}^{-1} \text{ K}^{-1}$ for the bulk thermal conductivity of SiO₂ to calculate the effective lattice thermal conductivity in two different heterostructures. In addition, we assume a uniform oxide-thickness during the whole oxidation process. The dotted curve corresponds to a single SiC layer on which a thin uniform SiO₂ film grows. For simplicity we assume that $p = 0$ at the SiO₂/SiC interface and

that the thickness $d_{\text{SiO}_2} + d_{\text{SiC}} = 200$ nm is kept fixed during the whole oxidation process that we model.⁷⁴ The solid (dashed) curve correspond to results for a doped-SiC/SiC/SiO₂ heterostructure evaluated under the assumption that $p = 1$ ($p = 0$) characterizes the scattering at the doped-SiC/SiC interface; we also assume that the underlying SiC layer is doped at a concentration of $5 \cdot 10^{19}$ cm⁻³. Our results document that the effective lattice thermal conductivity is sensitive to the oxide thickness and could be used as a qualitative in-situ probe of the SiC oxidation progress.⁴⁷

V. CONCLUSIONS

We have theoretically investigated the in-plane thermal transport in nanostructured semiconductor wires, layers and multilayers, in the framework of the l-BTE. The calculations include the important boundary scattering which specifies the phonon Knudsen flow and plays a dominant role in determining the thermal transport in semiconductor nanostructures. We obtain analytical results for the nanostructure thermal conductivity under the assumption of a frequency independent (constant) mean-free path ℓ_{mfp} . Our results further simplifies the thermal-transport calculations under more accurate assumptions for ℓ_{mfp} . We find that the lattice thermal conductivity is significantly suppressed from the bulk value at room temperature and below in both thin-wire and thin-layer nanostructures.

We have tested our approximative description of the phonon Knudsen flow effect by comparison to measurements of the thermal conductivity for thin Si wires and find that our analytical result for a constant ℓ_{mfp} provides a fair accuracy in a qualitative description. We further show that the traditional Fourier analysis³⁹ (typically used in finite-element calculations) predict an effective lattice thermal conductivity which is inaccurate for some nanostructured semiconductor systems especially in the low-temperature regime. Finally we have illustrated the use of the Knudsen-suppression thermal transport as a possible gauge of the SiC oxidation process.

Acknowledgments

We thank the National graduate school in materials science, the EU project ATOMCAD, and the Swedish Foundation for Strategic Research (SSF) though ATOMICS for support.

- ¹ G. Mahan, B. Sales, and J. Sharp, *Phys. Today* **50**, 42 (1997).
- ² D. G. Cahill, W. K. Ford, K. E. Goodson, G. Mahan, A. Majumdar, H. J. Maris, R. Merlin, and S. R. Phillpot, *J. Appl. Phys.* **93**, 793 (2003).
- ³ D. Li, Y. Wu, P. Kim, L. Shi, P. Yang, and A. Majumdar, *Appl. Phys. Lett.* **83**, 2934 (2003).
- ⁴ T. Yao, *Appl. Phys. Lett.* **51**, 1798 (1987).
- ⁵ T. S. Tighe, J. M. Worlock, and M. L. Roukes, *Appl. Phys. Lett.* **70**, 2687 (1997).
- ⁶ S.-M. Lee, D. G. Cahill, and R. Venkatasubramanian, *Appl. Phys. Lett.* **70**, 2957 (1997).
- ⁷ X. Y. Yu, G. Chen, A. Verma, and J. S. Smith, *Appl. Phys. Lett.* **67**, 3554 (1995).
- ⁸ D. G. Cahill, A. Bullen, and S.-M. Lee, *High Temperatures–High Pressures* **32**, 134 (2000).
- ⁹ K. Schwab, E. A. Henriksen, J. M. Worlock, and M. L. Roukes, *Nature* **404**, 974 (2000).
- ¹⁰ G. Chen, *J. Heat Transfer Trans.* **119**, 220 (1997).
- ¹¹ P. Hyldgaard and G. D. Mahan, *Thermal conductivity* (Technomic, Lancaster, PA 1996) **23**, 172 (1996).
- ¹² S. Y. Ren and J. Dow, *Phys. Rev. B* **25**, 3750 (1982).
- ¹³ P. Rennert and A. Brzezinski, *Phys. Rev. B* **52**, 1612 (1999).
- ¹⁴ A. Baladin and K. Wang, *Phys. Rev. B* **58**, 1544 (1998).
- ¹⁵ S. G. Walkauskas, D. A. Broido, and K. Kempa, *J. Appl. Phys.* **85**, 2579 (1999).
- ¹⁶ N. Mingo, L. Yang, D. Li, and A. Majumdar, *Nanoletters*, **3**, 1713 (2003).
- ¹⁷ X. Lü, W. Z. Shen, and J. H. Chu, *J. Appl. Phys.* **91**, 1542 (2002).
- ¹⁸ R. A. Richardson and F. Nori, *Phys. Rev. B* **48**, 15209 (1993).
- ¹⁹ J. Zou and A. Baladin, *J. Appl. Phys.* **89**, 2932 (2001).
- ²⁰ S. G. Volz and G. Chen, *Appl. Phys. Lett.* **75**, 2056 (1999).
- ²¹ N. Mingo and D. A. Broido, *Phys. Rev. Lett.* **93**, 246106 (2004).
- ²² L. Xiang, G. Ji-Hua, and C. Jun-Hao, *Chinese Physics* **10**, 223 (2001).
- ²³ A. I. Chervanyov, *Phys. Rev. B* **66**, 214302 (2002).

- ²⁴ X. Lü, J. H. Chu, W. Z. Shen, J. Appl. Phys. **93**, 1219 (2003).
- ²⁵ X. Lü and J. Chu, Phys. Stat. Sol. (b) **226**, 285 (2001).
- ²⁶ P. Chantrenne and J-L. Barrat, J. Heat Transfer Trans. **126**, 577 (2004).
- ²⁷ G. Chen, Phys. Rev. B **57**, 14958 (1998).
- ²⁸ P. Hyldgaard and G. D. Mahan, Phys. Rev. B **56**, 10754 (1997).
- ²⁹ P. Hyldgaard, Phys. Rev. B **69**, 193305 (2004).
- ³⁰ D.A. Broido and T. L. Reinecke, Phys. Rev. B **70**, 081310 (2004).
- ³¹ S. Tamura, Y. Tanaka, H. J. Maris, Phys. Rev. B **60**, 2627 (1999).
- ³² G. Chen and M. Neagu, Appl. Phys. Lett. **71**, 2761 (1997).
- ³³ S. Volz, J-B. Saulnier, G. Chen, and P. Beauchamp, High Temperatures–High Pressures **32**, 709 (2000).
- ³⁴ W. E. Bies, H. Ehrenreich, and E. Runge, J. Appl. Phys. **91**, 2033 (2002).
- ³⁵ G. Chen, T. Zeng, T. Borca-Tasciuc, and D. Song, Materials Science and Engineering **A292**, 155 (2000).
- ³⁶ C. L. Tien and G. Chen, J. Heat Transfeer **116**, 799 (1994).
- ³⁷ K. Fuchs, Proc. Cambridge Philos. Soc. **34**, 100 (1938).
- ³⁸ H. Smith and H. Højgaard Jensen, *Transport Phenomena* (Clarendon press, Oxford, 1989) pp. 246–257.
- ³⁹ E. Kreyszig, *Advanced Engeneering Mathematics* 8th Ed (Wiley, New York, 1999), ch 10.
- ⁴⁰ G. D. Mahan and L. M. Woods, Phys. Rev. Lett. **80**, 4016 (1998).
- ⁴¹ L. D. Hicks and M. S. Dresselhaus, Phys. Rev. B **47**, 12727 (1993).
- ⁴² G. D. Mahan and H. B. Lyon, Jr., J. Appl. Phys. **76**, 1899 (1994).
- ⁴³ J. O. Sofo and G. D. Mahan, Appl. Phys. Lett. **65**, 2690 (1994).
- ⁴⁴ D. A. Broido and T. L. Reinecke, Phys. Rev. B **51**, 13797 (1995).
- ⁴⁵ P. J. Lin-Chung and T. L. Reinecke, Phys. Rev. B **51**, 13244 (1995).
- ⁴⁶ D. A. Broido and T. L. Reinecke, Appl. Phys. Lett. **67**, 1170 (1995).
- ⁴⁷ E. Ziambaras and P. Hyldgaard, A brief report of selected multilayer transport results has been submitted as a conference proceedings; `cond-mat/0407122`.
- ⁴⁸ R. Rurali and N. Lorente, Phys. Rev. Lett. **94**, 026805 (2005).
- ⁴⁹ In fact, our analytical results for the wire and layer/multilayer Knudsen-flow suppression apply for transport of general quasiparticles with an isotropic dispersion assuming that the quasipar-

ticles can be ascribed a constant mean free path. Our analytical results should thus be directly applicable also for electronic transport in, for example, thin simple- and noble-metal films and wires.

- ⁵⁰ E. Ziambaras, Licentiate thesis, Chalmers University of Technology, (2004).
- ⁵¹ E. Ziambaras, in preparation.
- ⁵² *Landolt-Börnstein: Numerical Data and Functional Relationships in Science and Technology*, edited by O. Madelung, New Series, Group III, Vol. 41A1a (Springer, Berlin, 2001).
- ⁵³ D. W. Feldman, J. H. Parker, W. Choyke, and L. Patrick, *Phys. Rev.* **173**, 787 (1968).
- ⁵⁴ The parameters α_i are obtained from $\alpha_i = (q_{\max}c_i/\omega(q_{\max}) - 1)/\omega^3(q_{\max})$ to fit the energies at the zone boundaries $\Theta_i = \hbar\omega(q_{\max})/k_B$ which are estimated from the phonon dispersion curves in Ref. 52.
- ⁵⁵ J. M. Ziman, *Electrons and Phonons* (Oxford University Press, Oxford, 1960), p. 264.
- ⁵⁶ G. A. Slack, *J. Appl. Phys.* **35**, 3460 (1964).
- ⁵⁷ A. P. Prudnikov, Yu. A. Brychkov, O. I. Marichev, *Integrals and Series*, Vol. 3: More special functions, (Gordon and Breach, New York, 1990).
- ⁵⁸ Our result (21) disagrees, however, with the formal result, Eqs. (7)–(9), of Ref. 15 and we suspect a simple typo in their Eq. (7) that yields negative results for the thermal conductivity in very thin wires.
- ⁵⁹ M. I. Flik and C. L. Tien, *J. Heat Transfer* **112**, 872 (1990).
- ⁶⁰ J. Tan, M. K. Das, J. A. Cooper, Jr. and M. R. Melloch, *Appl. Phys. Lett.* **70**, 2280 (1997).
- ⁶¹ M. DiVentra and S. Pantelides, *Phys. Rev. Lett.* **83**, 1624 (1999).
- ⁶² A. Gali, D. Heringer, P. Deák, Z. Hajnal, Th. Frauenheim, R. P. Devaty, and W. J. Choyke, *Phys. Rev. B* **66**, 125208 (2002).
- ⁶³ M. DiVentra and S. Pantelides, *Phys. Rev. Lett.* **86**, 5946 (2001).
- ⁶⁴ P. Deák, A. Gali, Z. Hajnal, Th. Frauenheim, N. T. Son, E. Janzén, and W. J. Choyke, *Mat. Sci. Forum* **433-436**, 535 (2003).
- ⁶⁵ R. Rurali, E. Wachowicz, P. Ordejon, P. Godignon, J. Rebollo, and P. Hyldgaard, *Mat. Sci. Forum* **457-460**, 1293 (2004).
- ⁶⁶ E. Wachowicz, R. Rurali, P. Ordejon, and P. Hyldgaard, *Comp. Mat. Sci.* **33**, 13 (2005).
- ⁶⁷ R. Duś, E. Nowicka, and R. Nowakowski, *Langmuir* **20**, 9138 (2004).
- ⁶⁸ G. Palasantzas, Y.-P. Zhao, G.-C. Wang, T.-M. Lu, J. Barnas, and J. Th. M. De Hosson, *Phys.*

Rev. B **61**, 11109 (2000).

⁶⁹ E. Z. Luo, S. Heun, M. Kennedy, J. Wollschläger, and M. Henzler, Phys. Rev. B **49**, 4858 (1994).

⁷⁰ S. Kumar and G. C. Vradis, J. Heat Transfer Trans. **116**, 28 (1994).

⁷¹ H. Grabhorn, A. Otto, D. Schumacher, and B.N.J. Persson, Surf. Sci. **264**, 327 (1992).

⁷² R. Duś, private communication.

⁷³ M. G. Burzo, P. L. Komarov, and P. E. Raad, IEEE Trans. Comp. Pack. Tech. **26**, 80 (2003).

⁷⁴ In typical experiments the final oxide thickness is about two times the starting silicon thickness, Ref. 60, but that complication has no effect on the present conclusions due to the vanishing contribution of the SiO₂ to the overall thermal conduction.

TABLES

TABLE I: Model parameters of the phonon description in SiC, Si, GaAs, and Ge. The measured longitudinal and transverse sound velocities, c_l and c_t , in SiC are taken from Ref. 53 while for Si, GaAs, and Ge we use Ref. 52. The Debye temperatures, Θ_l and Θ_t , are defined as $\Theta_i = \hbar\omega_i(q_{\max})/k_B$ and have in all four cases been calculated from the phonon dispersion curves in Ref. 52.

| Material | c_l | c_t | Θ_l | Θ_t | $\alpha_l\omega_l^3(q_{\max})$ | $\alpha_t\omega_t^3(q_{\max})$ |
|----------|-------|-------|------------|------------|--------------------------------|--------------------------------|
| SiC | 13300 | 7250 | 880 | 380 | 0.72 | 1.23 |
| Si | 8480 | 5870 | 570 | 160 | 0.43 | 1.91 |
| Ge | 4960 | 3570 | 360 | 120 | 0.20 | 1.51 |
| GaAs | 4730 | 3340 | 270 | 100 | 0.55 | 1.95 |

FIGURES

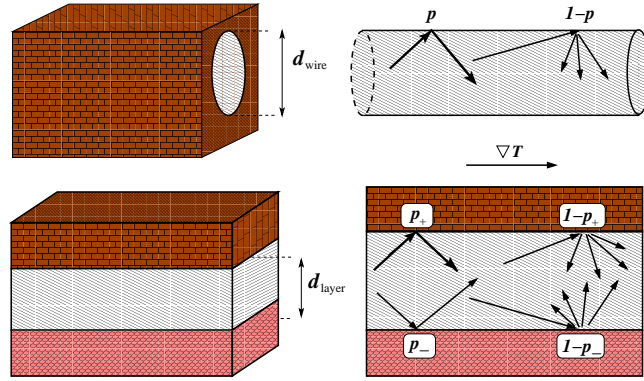


FIG. 1: Typical semiconductor nanostructures that are subject to a Knudsen-flow effect (Refs. 37 and 38) with a suppression of the thermal conductivity. Phonon transport can be effectively confined to device channels (light gray) by the low conductivity of the processed surrounding. Moreover this in-channel thermal transport typically suffers a significant suppression by interface scattering. The upper panel illustrates two possible realizations of a wire which could be embedded in an oxide or free-standing. Phonons experience specular (diffusive) scattering with the probability p ($1-p$) at the wire boundaries. The lower panel shows a corresponding realization of a multilayered nanostructure in which, for example, a transport channel is located between two (in general) different materials (for example, a top oxide and a heavily doped substrate). Phonons scatter specularly from the upper (lower) interface with probability $p_{+(-)}$ and diffusively with probability $1 - p_{+(-)}$ to produce a Knudsen flow.

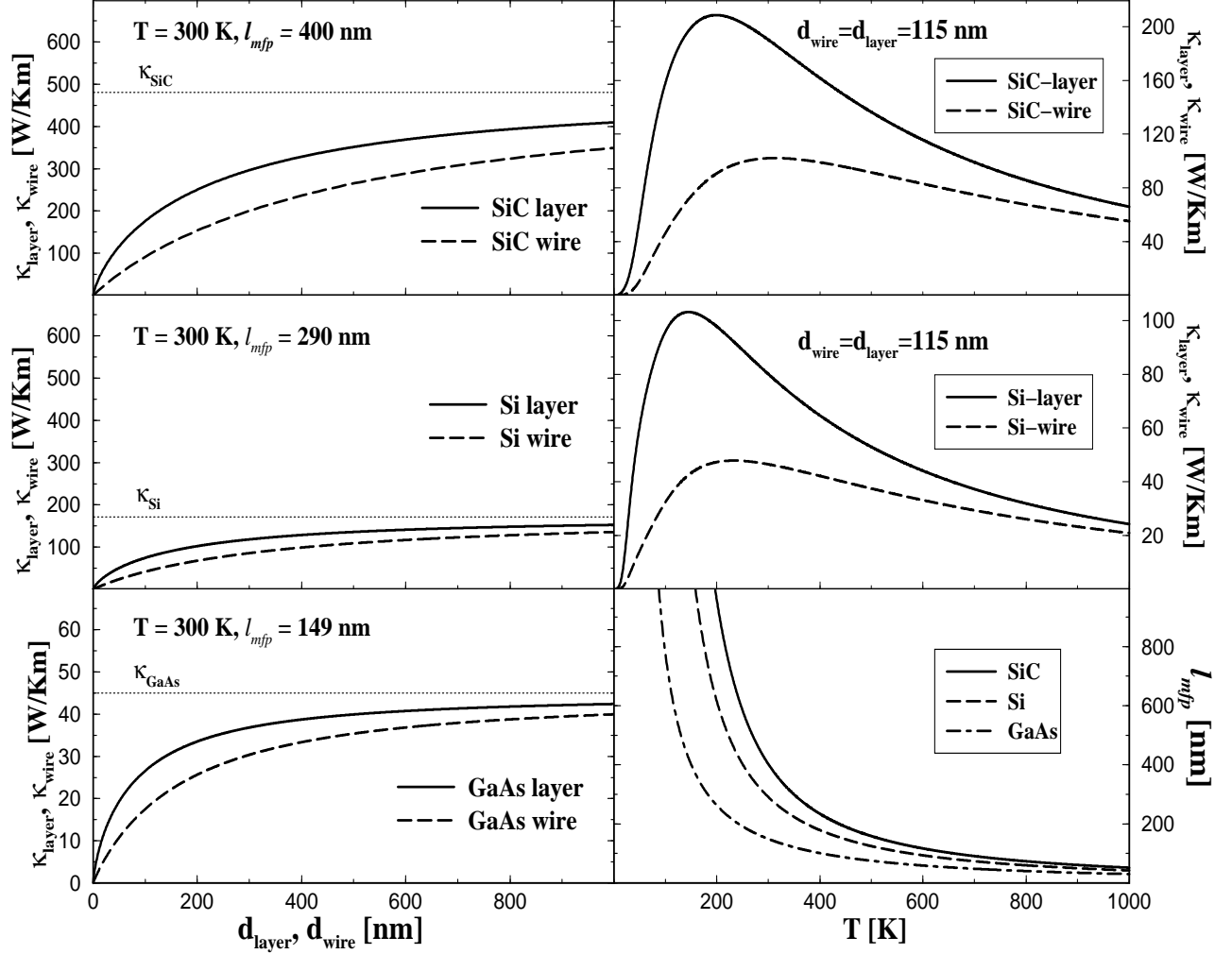


FIG. 2: Summary and origin of predicted suppression in the thermal conductivity of nanostructured semiconductor structures. *The left panels* show the thermal conductivity of layer (solid curves) and wire (dashed curves) structures calculated as a function of the layer thickness and wire diameter at room temperatures for three typical semiconductor materials. The dotted lines identifies the experimentally observed value of the bulk-material thermal conductivities from which we also extract the listed values of the phonon mean free paths ℓ_{mfp} . A corresponding graph for Ge gives almost similar values to that of GaAs. *The right top and right middle panels* compare the predicted temperature variation of the layer and wire thermal conductivity in SiC and Si for a layer thicknesses d_{layer} /wire diameter d_{wire} for which there now exist experimental realizations as Si nanowires (Ref. 3). *Finally, the lower right panel* shows the calculated temperature variation in the almost micron-scale phonon mean free paths in bulk SiC, Si, and GaAs. The predicted phonon mean free path exceeds the typical separation between material interfaces in nanostructures and explains the device importance of the phonon Knudsen flow effect.

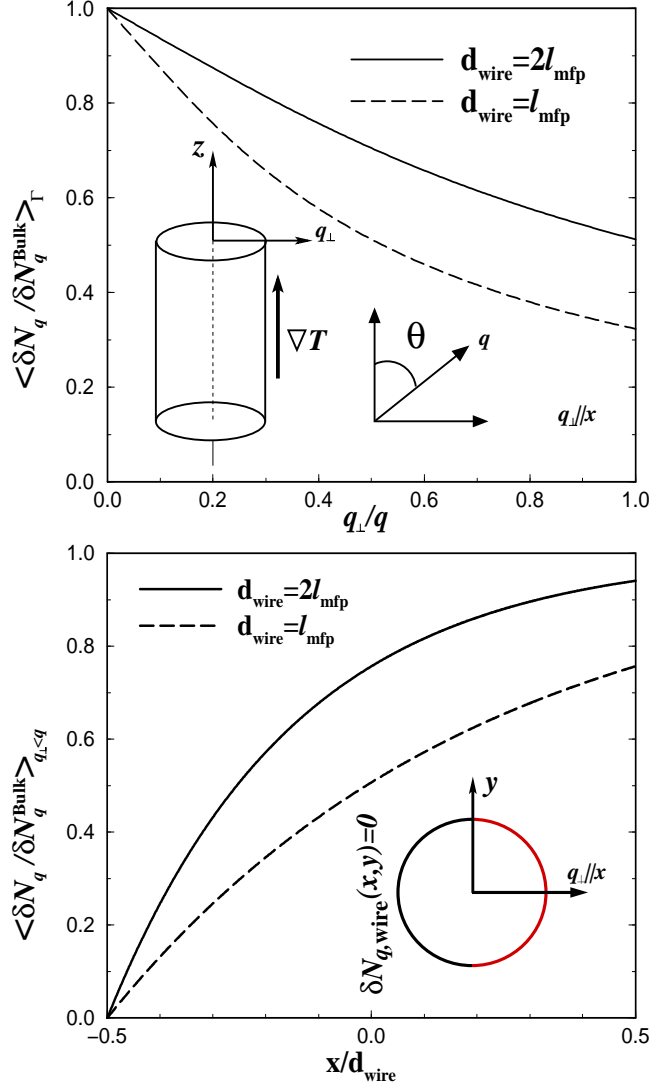


FIG. 3: Schematics and details of the Knudsen-flow effect as expressed in the momentum and spatial variation in the thermal-gradient induced changes in the phonon distribution. The figure shows (for a given magnitude q of the phonon momentum \mathbf{q}) the ratio of the distribution change $\delta N_q = \delta N_q^{\text{wire}}$ (arising in a wire with purely diffusive interface scattering) to the corresponding bulk-distribution changes δN_q^{Bulk} evaluated for different ratios of $d_{\text{wire}}/\ell_{\text{mfp}}(q)$. *The top panel* shows this distribution ratio (averaged over the wire cross section) as a function of the angle θ between the phonon momentum and the wire axis/thermal-gradient direction/transport direction z . *The bottom panel* shows the corresponding variation of the distribution ratio (averaged over θ) with the coordinate x (at $y = 0$) along the wire diameter which is assumed to coincide with the direction of the perpendicular momentum component q_\perp .

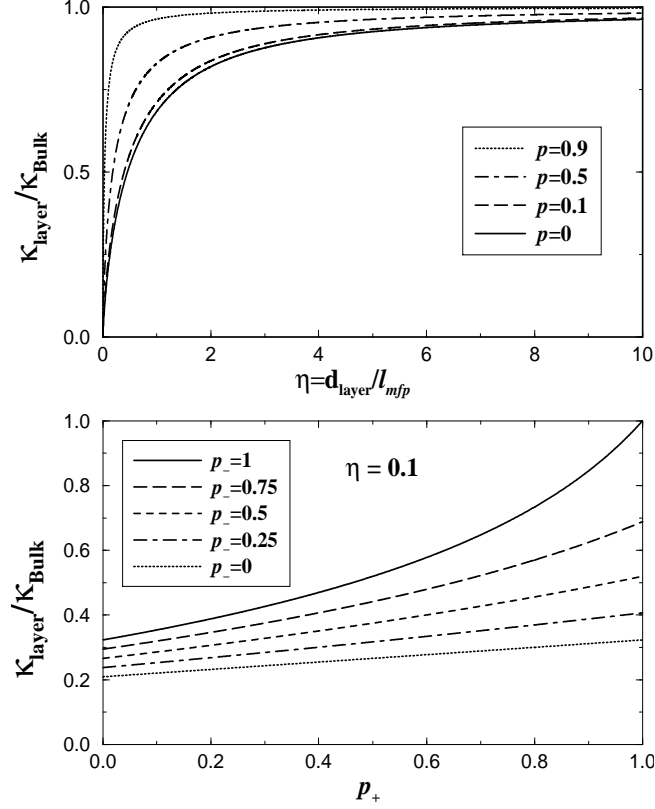


FIG. 4: Relative suppression of the thermal conductivity in a general individual semiconductor layer evaluated for a the constant mean free path ℓ_{mfp} . *The upper panel* shows the thermal conductivity ratios, $\kappa_{\text{layer}}/\kappa_{\text{Bulk}}$, as a function of η for specular scattering probabilities $p_+ = p_- = p$. The thermal conductivity naturally increases to recover the bulk-like behavior recovers when the probability for specular scattering increases. *The lower panel* shows the ratio $\kappa_{\text{layer}}/\kappa_{\text{Bulk}}$ as a function of p_+ for different p_- evaluated at a given ratio $\eta = d_{\text{layer}}/\ell_{\text{mfp}} = 0.1$. The panel documents that the layer thermal conductivity remains significantly suppressed from the bulk transport value even when the phonons scatter purely specularly ($p_{\pm} = 1$) from one of the interfaces.

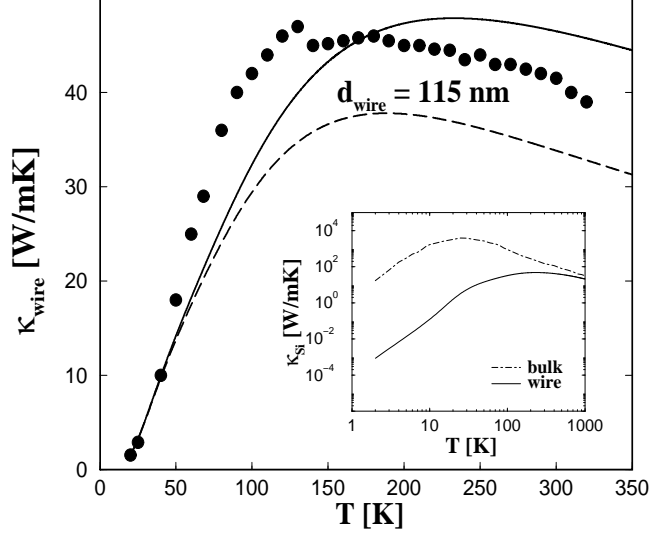


FIG. 5: Test of accuracy of our approximative phonon Knudsen flow description. The figure shows the temperature variation of the lattice thermal conductivity in a 115 nm thick silicon wire. The solid circles represent experimental values from Ref. 3. The dashed (solid) curve shows our theory estimate for pure diffusive scattering, $p = 0$, and calculated assuming a frequency-dependent relaxation time¹⁵ $\tau_q = A(T)/\omega_q^2$ (a frequency-/polarization-independent bulk-phonon mean free path $\ell_{\text{mfp}}(T)$ specified by bulk-measurements.) The inset compares the temperature-variation on logarithmic scales of bulk-Si thermal transport (dashed-dotted curve) and the evaluated Si-wire conductivity (solid curve) calculated for a frequency-independent $\ell_{\text{mfp}}(T)$.

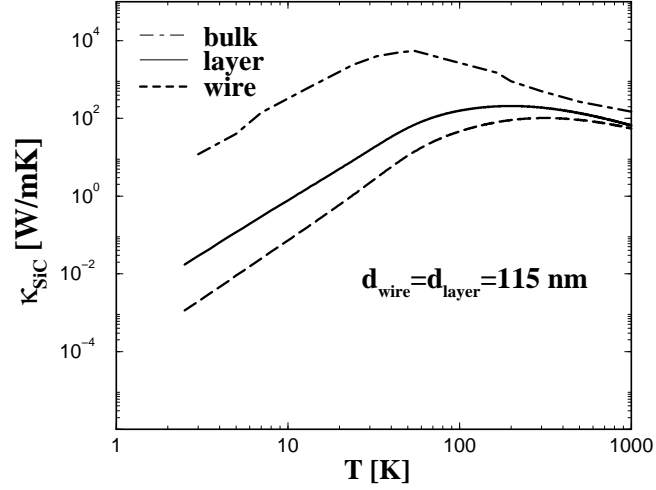


FIG. 6: Thermal conductivity suppression in 115 nm thick SiC wires (dashed curve) and layers (solid curve) compared to the bulk-SiC thermal conductivity measurements (dashed-dotted curve).⁵⁶ The peak values for the wire and layer transport case are about two orders of magnitude smaller than the bulk-transport peak and are shifted to much higher temperatures.

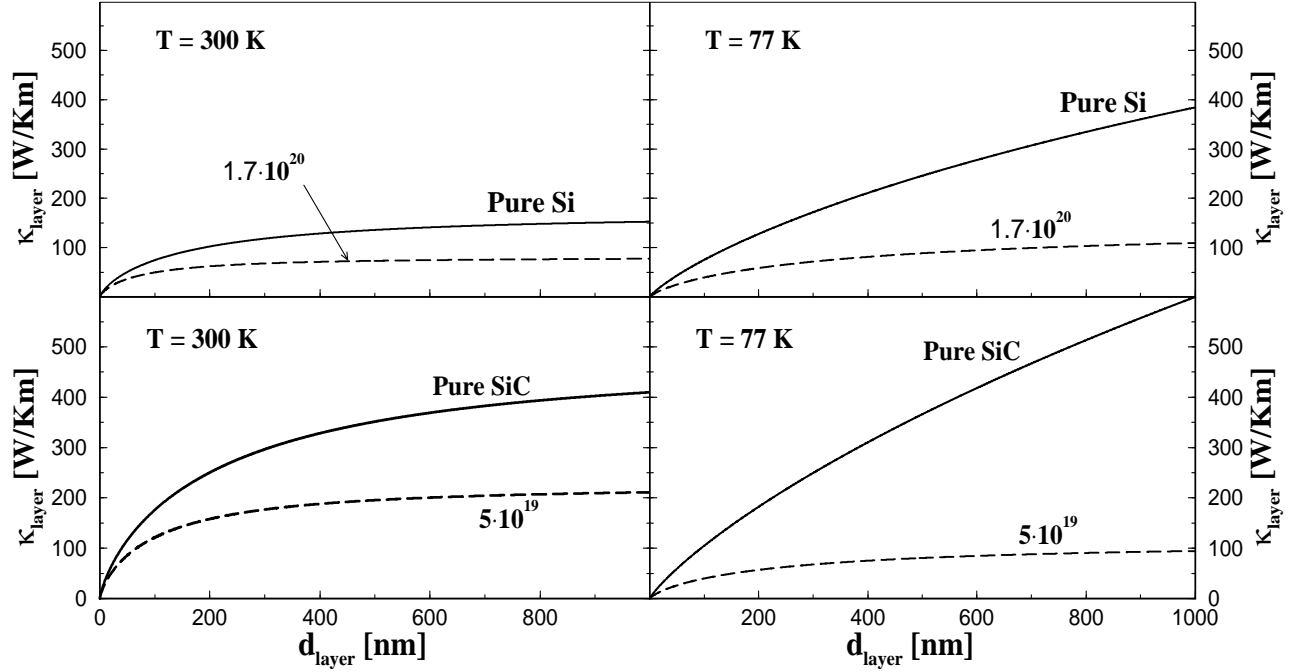


FIG. 7: Reduction of the lattice thermal conductivity in doped and undoped layers of Si (top panels) and SiC (bottom panels). In all four panels the lattice thermal conductivity, κ_{layer} , is plotted as a function of the layer-thickness, d_{layer} , for $p_+ = p_- = 0$ at $T = 300$ K (left panels) and $T = 77$ K (right panels). The *top panels* show κ_{layer} in pure (solid curves) and in p-doped (dashed curves) Si layers. Similarly, the *bottom panels* compare the lattice thermal conductivity in pure SiC layers (solid curves) to that of n-doped layers (dashed curves).

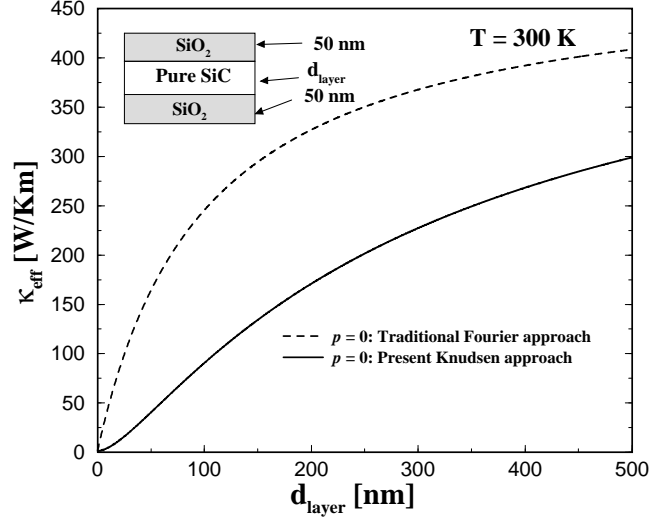


FIG. 8: Comparison of traditional thermal-transport calculations³⁹ (dashed curve) and present Knudsen-flow results (solid curve), Eqs. (31) and (24)–(29). The panel shows the effective lattice thermal conductivity as a function of the layer thickness in a SiC layer that is located between two 50 nm thick SiO₂ layers. The traditional thermal-transport calculations overestimates the thermal conductivity significantly in low-dimensional semiconductor structures at room temperatures and below. The figure therefore suggests a breakdown of the Fourier approach based on bulk conductivities as in typically used in finite-element calculations.

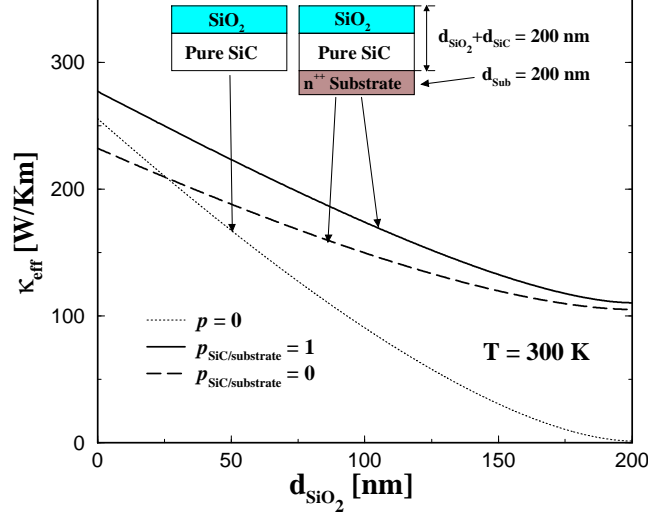


FIG. 9: Possible probe of the SiC oxidation process as measured by the variation in the effective lattice thermal conductivity with the oxide-thickness, d_{SiO_2} . The dotted curve correspond to a single SiC layer on which a thin uniform SiO₂ film grows. The solid (dashed) curve shows results for a doped-SiC/SiC/SiO₂ heterostructure evaluated under the assumption that $p = 1$ ($p = 0$) characterize the scattering at doped-SiC/SiC interface and $p = 0$ characterize the SiO₂/SiC interface. We assume that the underlying SiC layer is doped at a concentration of $5 \cdot 10^{19} \text{ cm}^{-3}$. For simplicity we also assume that the thickness $d_{\text{SiO}_2} + d_{\text{SiC}} = 200 \text{ nm}$ is kept fixed during the whole oxidation process that we model⁷⁴.